Renormalization and damping of dipole-exchange spin waves in ultrathin antiferromagnetic films

J. Milton Pereira, Jr.[1,2] and M. G. Cottam[2]
[1]*Departamento de Física, Universidade Federal do Ceará, Fortaleza, Ceará, 60455-760, Brazil*
[2]*Department of Physics and Astronomy, University of Western Ontario, London, Ontario, N6A 3K7, Canada*
(Received 14 March 2003; published 25 September 2003)

The damping and frequency shift of spin wave modes due to magnon-magnon interactions in ultrathin antiferromagnetic films are studied in the dipole-exchange regime. We employ a Hamiltonian formalism that uses a transformation of the spin operators to boson operators in the film geometry and calculate the effects of the three- and four-magnon interactions on the spin wave spectrum by means of a diagrammatic perturbation technique. With this formalism we obtain expressions for the damping and energy shift of the discrete spin wave modes in bcc antiferromagnetic films as a function of wave vector and temperature. Numerical results are shown for ultrathin films of the antiferromagnet MnF_2.

DOI: 10.1103/PhysRevB.68.104429 PACS number(s): 75.30.Ds, 75.70.−i

I. INTRODUCTION

The study of low-dimensional systems is currently one of the most fruitful areas of research in solid state physics. This is a consequence of the great variety of such systems, their relation with new technological applications (especially in microelectronics), and also due to an increasing interest in understanding the basic physical processes in these systems, which, in general, consist of fabricated structures that may have no natural counterparts. The excitations in low-dimensional magnetic systems, in particular, can behave in a strikingly different way than their three-dimensional (3D) equivalents. There is an extensive body of work related to the properties of the spin wave (SW) excitations in magnetic systems of reduced dimensionality, e.g., films, superlattices, wires, and dots.[1–3]

In this work we present a study of interaction processes between the SW in ultrathin antiferromagnetic films. This description usually corresponds to films with a relatively low number of atomic layers (e.g., below 100). Most previous studies[4–6] of SW modes in ultrathin films have neglected higher-order SW effects, which, nevertheless, can become significant as the temperature of the system increases. The motivation for the present study is to extend previous calculations for the *linear* SW spectrum in antiferromagnetic films,[7] employing a theory for the interaction processes that builds upon a previous formalism for the study of nonlinear processes in ferromagnets.[8–10] The formalism is based on a microscopic description of the film, in which the position dependence of the magnetic sites in the medium is realistically taken into account. Our model includes the short-range exchange coupling (which dominates the SW dynamics at short wavelengths) as well as the long-range dipolar interaction between localized spins in the magnetic structure (which are increasingly important at longer wavelengths). The fact that the dipolar interaction has a much longer range than exchange coupling means that these interactions affect the SW dynamics in different ways. Most previous *microscopic* calculations for SW interactions in films have focused on situations where only the exchange interaction is important. However, this assumption may be unrealistic, especially when one is dealing with low-dimensional systems and/or small wave vectors. Existing works on magnetic waves in films with both dipole-dipole and exchange interactions have primarily considered *macroscopic* approximations, which treat the magnetic medium as an effective continuum (for a review see, e.g., Ref. 2). These macroscopic models are expected to break down in the case of larger wave vectors and/or very thin films. On the other hand, by using a microscopic description one can obtain dispersion relations of the discrete SW modes for ultrathin samples and for the whole Brillouin zone. The limitations of the macroscopic theories can also be tested.

In antiferromagnetic films the existence of two sublattices tends to increase the complexity of the analytical expressions, compared with the ferromagnetic case. On the other hand, it also raises the possibility of a wider variety of nonlinear effects. In addition, antiferromagnets usually have a richer spectrum of excitations due to the different spin ordering, and the SW frequency range is typically different (i.e., in the infrared instead of the microwave region). As we show below for the case of antiferromagnets with a body-centered cubic or tetragonal structure, the complexity of the equations describing the different SW interaction processes can be significantly reduced by means of a simple mathematical transformation.

The inclusion of interaction processes in the theory may result in the occurrence of a frequency shift and damping of the SW modes. These effects can be calculated by means of a diagrammatic perturbation technique. This method allows one to include in a rigorous fashion the effects of the different processes. In this paper we employed such a perturbative technique to obtain the energy shift and the damping by evaluating the proper self-energies for diagrams corresponding to three-magnon processes, which arise due to the dipolar interaction, as well as for diagrams representing four-magnon processes, which contain contributions from both exchange and dipole-dipole couplings. Results are shown as a function of temperature and wave vector.

The corresponding treatment of three-magnon and four-magnon processes in bulk (i.e., effectively infinite) dipolar antiferromagnets, using a microscopic (or Hamiltonian) approach, is well known (see, e.g., Refs. 11 and 12). The essential differences in our present work on thin films arise

from the quantization of the SW spectra and the truncation of the dipole-dipole interactions due to the surfaces.

This paper is arranged as follows. Section II gives a description of the microscopic Hamiltonian formalism, including the dipolar and exchange terms. An expansion in terms of boson operators is made, generalizing the method described in Refs. 9 and 10, and some results for the linear SW spectrum are briefly discussed. The following sections are devoted to an analysis of the higher-order (nonlinear SW) terms in the Hamiltonian using a Green's function diagrammatic formalism. The terms corresponding to three- and four-magnon processes are discussed in Secs. III and IV, respectively. In both cases the energy shift and damping of each discrete SW mode are deduced from the relevant proper self-energies. In Sec. V the numerical results with application to MnF_2 are discussed, and finally the conclusions are presented in Sec. VI.

II. THE HAMILTONIAN

The system consists of a two-sublattice antiferromagnetic thin film that has N atomic layers. The external magnetic field of magnitude H_0 is parallel to the surface, along the z axis, taken as the axis of sublattice magnetization. We assume that the film has a bcc or tetragonal structure (e.g., as for the magnetic ions in MnF_2 or FeF_2) and that the surfaces correspond to a (100) crystal plane. The Hamiltonian is written as

$$H=\sum_{i,j} J_{ij}\mathbf{S}_i\cdot\mathbf{S}_j-g\mu_B\sum_i (H_0+H_{Ai})S_i^z$$

$$-\sum_j g\mu_B(H_0-H_{Aj})S_j^z+g^2\mu_B^2\sum_{\alpha,\beta}\sum_{l,m} D_{lm}^{\alpha\beta}S_l^\alpha S_m^\beta, \quad (1)$$

where J_{ij} is the exchange coupling between nearest-neighbor sites and $H_{Ai,j}$ are effective anisotropy fields. The i (j) indices correspond to sites in the sublattice of up (down) spins. We note that, in this geometry, each layer consists of spins of one sublattice type only (see Fig. 1). The exchange constant is assumed to have a value J when connecting magnetic sites in the interior of the film, and J_S when both interacting sites are located on the surface. The last term in Eq. (1) contains the contribution of the dipolar interaction. Since this is a long-range coupling, the summations over l and m run over all the sites. The α and β indices denote components x, y, or z, while g is the Landé factor and μ_B is the Bohr magneton. The expression for the factors $D_{lm}^{\alpha\beta}$ is

$$D_{lm}^{\alpha\beta}=\frac{[|\mathbf{r}_{lm}|^2\delta_{\alpha\beta}-3r_{lm}^\alpha r_{lm}^\beta]}{|\mathbf{r}_{lm}|^5}, \quad (2)$$

where the vector $\mathbf{r}_{lm}=\mathbf{r}_l-\mathbf{r}_m$ connects magnetic sites in the lattice. This term will be multiplied by $\frac{1}{2}$ when it involves pairs of spins on the same sublattice to prevent double counting.

The spin Hamiltonian can be rewritten in terms of boson creation and annihilation operators. This mapping can be done according to several schemes and in the present case we use the Holstein-Primakoff transformation (e.g., as in Ref. 10):

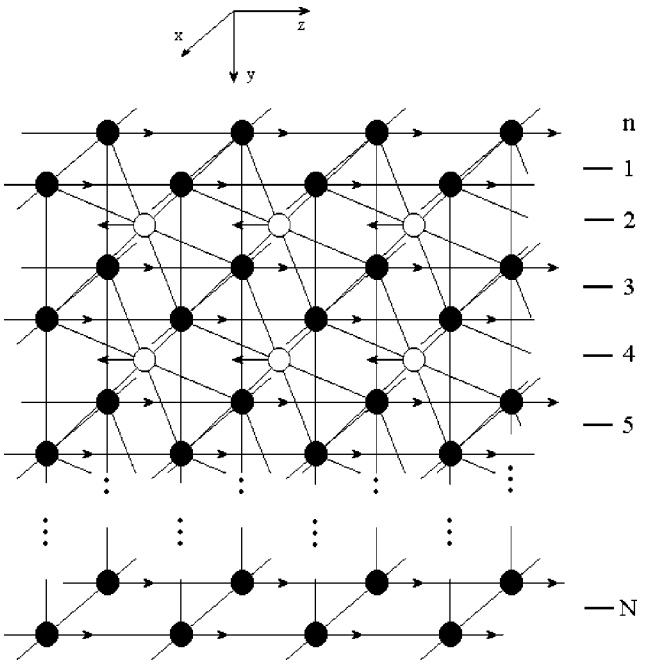

FIG. 1. Schematic view of a N-layer antiferromagnetic film with body-centered structure, showing the choice of coordinate axes.

$$S_i^+=\sqrt{2S}\left[\sqrt{1-\frac{a_i^\dagger a_i}{2S}}\right]a_i, \quad (3)$$

$$S_i^-=\sqrt{2S}a_i^\dagger\left[\sqrt{1-\frac{a_i^\dagger a_i}{2S}}\right], \quad (4)$$

$$S_i^z=S-a_i^\dagger a_i \quad (5)$$

for the S_i (spin-up) operators and

$$S_j^+=\sqrt{2S}b_j^\dagger\left[\sqrt{1-\frac{b_j^\dagger b_j}{2S}}\right], \quad (6)$$

$$S_j^-=\sqrt{2S}\left[\sqrt{1-\frac{b_j^\dagger b_j}{2S}}\right]b_j, \quad (7)$$

$$S_j^z=-S+b_j^\dagger b_j \quad (8)$$

for the S_j (spin-down) operators. The transformed Hamiltonian can then be expanded (apart from a constant) as

$$H=H^{(1)}+{}^{(2)}+H^{(3)}+H^{(4)}+\cdots, \quad (9)$$

where $H^{(p)}$ (with $p=1,2,\ldots$) denotes the term involving a product of p boson operators. The $H^{(1)}$ term can be shown to vanish due to symmetry for the lattice types under consideration. The bilinear term $H^{(2)}$ describes the noninteracting (linear) SW modes in the system while the other terms in the Hamiltonian represent the leading-order contributions involving SW interactions.

The $H^{(2)}$ term in the Hamiltonian for the assumed antiferromagnet is given, using a representation in terms of a 2D (in-plane) wave vector $\mathbf{k}=(k_x,k_z)$ and a layer index n $(=1,2,\ldots,N)$, by

$$H^{(2)}=\sum_{\mathbf{k},n,n'}\{M_{n,n'}(\mathbf{k})c^{\dagger}_{\mathbf{k}n}c_{\mathbf{k}n'} + N_{n,n'}(\mathbf{k})[c_{\mathbf{k}n}c_{-\mathbf{k}n'}+c^{\dagger}_{\mathbf{k}n}c^{\dagger}_{-\mathbf{k}n'}]\}, \tag{10}$$

where the c operators are defined as

$$c_{\mathbf{k}n}=\begin{cases} a_{\mathbf{k}n}, & n=2l-1, \\ b^{\dagger}_{\mathbf{k}n}, & n=2l,\ \ l=1,2,\ldots . \end{cases} \tag{11}$$

The c operators must then obey the commutation relation

$$[c_{\mathbf{k}n},c^{\dagger}_{\mathbf{k}'n'}]=(-1)^{n+1}\delta_{n,n'}\delta_{\mathbf{k},\mathbf{k}'}. \tag{12}$$

Also, in Eq. (10), we define

$$M_{n,n'}(\mathbf{k})=\Bigg\{g\mu_B H_{(n)}+S\Bigg[v_{n,n+1}(0)+v_{n,n-1}(0) + \sum_{n''}(-1)^{n-n''}(g\mu_B)^2 D^{zz}_{n,n''}(0)\Bigg]\Bigg\}\delta_{n,n'} + S\Bigg[v_{n,n-1}(\mathbf{k})\delta_{n',n-1}+v_{n,n+1}(\mathbf{k})\delta_{n',n+1} - \frac{1}{2}(g\mu_B)^2 D^{zz}_{n,n'}(\mathbf{k})\Bigg] \tag{13}$$

and

$$N_{n,n'}=\frac{1}{4}S(g\mu_B)^2[D^{xx}_{n,n'}(\mathbf{k})-D^{yy}_{n,n'}(\mathbf{k})-2iD^{xy}_{n,n'}(\mathbf{k})], \tag{14}$$

where $H_{(n)}=H_0-(-1)^n H_A$, $v_{n,n\pm1}(\mathbf{k})=4J\cos(k_x a/2)\times\cos(k_z a/2)$, and $D^{\alpha\beta}_{n,n'}(\mathbf{k})$ are Fourier transforms of the dipolar interactions defined in Eq. (2).

The next step, before proceeding to include the higher-order Hamiltonian terms, is to diagonalize $H^{(2)}$. By analogy with Refs. 9 and 10, this will have the effect of ''projecting out'' the linear SW modes. We recall that in an antiferromagnetic film with N layers there are N SW modes, and these occur in doubly degenerate pairs. We assign an index ν $(=1,2,\ldots,N)$ to each SW mode with energy $\epsilon_\nu(\mathbf{k})$ at 2D wave vector $\mathbf{k}$, and then we perform a simple canonical transformation on the c operators that diagonalizes the bilinear part of the Hamiltonian as a function of boson creation and annihilation operators (see the Appendix). The $H^{(2)}$ part of the Hamiltonian can then be rewritten as a function of the transformed operators (denoted by $\alpha^{\dagger}$ and α) as

$$H^{(2)}=-\frac{1}{2}\sum_{\mathbf{k},n}[M_{n,n'}(\mathbf{k})(-1)^n-\boldsymbol{\varepsilon}(\mathbf{k})]\delta_{n,n'} + \sum_{\mathbf{k},\nu}\epsilon_\nu(\mathbf{k})\alpha^{\dagger}_{\mathbf{k},\nu}\alpha_{\mathbf{k},\nu}. \tag{15}$$

Thus the linear SW spectrum can be found by evaluating the $\epsilon_\nu(\mathbf{k})$ factors. Some results for the linear SW spectrum in bcc antiferromagnetic thin films have been published previously.[7] We now focus on the higher-order terms in the expansion of the Hamiltonian.

III. THREE-MAGNON PROCESSES

The terms that contain products of three boson operators are specifically due to the dipolar interaction, and originate from spin products of the types S^xS^z, S^yS^z, etc., in the original Hamiltonian. Their contribution can be written, in terms of the in-plane wave vector and layer indices, as

$$H^{(3)}=\frac{1}{2}\sum_{\mathbf{k},\mathbf{q},n,n'}F_{nn'}(\mathbf{k})(c_{\mathbf{k}n}c^{\dagger}_{\mathbf{q}n'}c_{\mathbf{q}-\mathbf{k}n'}+c^{\dagger}_{\mathbf{k}n}c^{\dagger}_{\mathbf{q}-\mathbf{k}n'}c_{\mathbf{q}n'}), \tag{16}$$

where

$$F_{nn'}(\mathbf{k})=(-1)^{n'+1}(g\mu_B)^2(2S)^{1/2}[D^{xz}_{nn'}(\mathbf{k})-iD^{yz}_{nn'}(\mathbf{k})]. \tag{17}$$

This equation has a form similar to that in Ref. 10 for the simple cubic ferromagnet. In the present case the information relating to the two-sublattice structure is implicit in our expression for the interaction potential.

It is now necessary to rewrite Eq. (16) in terms of the α and $\alpha^{\dagger}$ operators that diagonalize the bilinear part of the Hamiltonian, as described previously. Under this transformation the $H^{(3)}$ term is found to contain four different combinations of products of these operators, and can be expressed as

$$H^{(3)}=\frac{1}{2}\sum_{l_1l_2l_3\mathbf{k}\cdot\mathbf{q}}[V_1\alpha^{\dagger}_{\mathbf{k},l_1}\alpha^{\dagger}_{\mathbf{q}-\mathbf{k},l_2}\alpha_{\mathbf{q},l_3}+V_2\alpha^{\dagger}_{\mathbf{q},l_1}\alpha_{\mathbf{q}-\mathbf{k},l_2}\alpha_{\mathbf{k},l_3} + V_3\alpha^{\dagger}_{\mathbf{k},l_1}\alpha^{\dagger}_{\mathbf{q}-\mathbf{k},l_2}\alpha^{\dagger}_{-\mathbf{q},l_3}+V_4\alpha_{-\mathbf{q},l_1}\alpha_{\mathbf{q}-\mathbf{k},l_2}\alpha_{\mathbf{k},l_3}]. \tag{18}$$

The V_i $(i=1,2,3,4)$ coefficients are the canonically transformed interaction potentials for each term. They are given formally by the same expressions as in Ref. 10 [but using the redefined $F_{nn'}(\mathbf{k})$ and canonical transformation matrices for the antiferromagnetic case], and so will not be quoted here. These coefficients (and likewise those in the next section for the four-magnon processes) are the analogs of coefficients introduced by L'vov[12] for bulk antiferromagnets. However, they depend on additional indices due to the discrete nature of the SW spectrum.

The terms in $H^{(3)}$ lead to a renormalization (i.e., an energy shift and damping) of the SW modes. The processes can be represented diagrammatically by closely following the notation and procedure used recently for ultrathin ferromag-

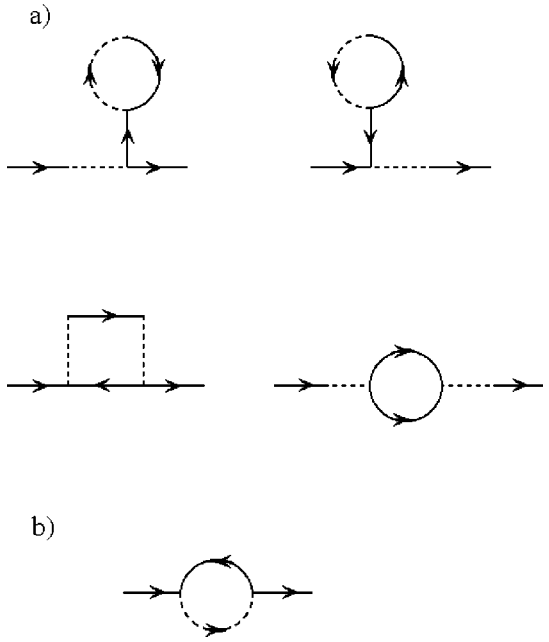

FIG. 2. Topological form of the proper self-energy diagrams resulting from (a) three-magnon and (b) four-magnon interaction processes in leading order.

netic films.[10] The corresponding diagrammatic vertices consist an interaction V_i and two SW lines entering or leaving. The lines represent the Green's functions for the propagation of a linear SW from any branch and with any 2D wave vector: in our case they can be deduced from Eq. (15) for the noninteracting Hamiltonian $H^{(2)}$ in its diagonalized form. The SW modes that are involved in the $H^{(3)}$ interaction vertices may be from the same or different branches. Since these terms have an odd number of operators, the leading-order contributions to the required proper self-energies (to renormalize the SW Green's functions) are necessarily of second order in the V_i factors [see Fig. 2(a), where the topological form of the self energy diagrams are illustrated]. The SW energy shift and damping are related to the real and imaginary parts, respectively.[10] In the case of antiferromagnetic films we eventually obtain the following expression for the energy shift due to three-magnon processes:

$$\Delta\epsilon_{\mathbf{q},l}=P\sum_{\mathbf{q}'l'l''}\left\{(W_a+W_b)\frac{n^0(\epsilon_{\mathbf{q}',l'})}{\epsilon_{\mathbf{q},l''}}\right.$$
$$+W_c\frac{n^0(E_{\mathbf{q}'l'})+n^0(\epsilon_{-\mathbf{q}-\mathbf{q}',l''})+1}{\epsilon_{-\mathbf{q}-\mathbf{q}',l''}+\epsilon_{\mathbf{q}',l'}+\epsilon_{\mathbf{q},l}}$$
$$+W_d\frac{n^0(\epsilon_{\mathbf{q}'l'})+n^0(\epsilon_{\mathbf{q}-\mathbf{q}',l''})+1}{\epsilon_{\mathbf{q}-\mathbf{q}',l''}+\epsilon_{\mathbf{q}',l'}-\epsilon_{\mathbf{q},l}}$$
$$\left.+W_e\frac{n^0(\epsilon_{\mathbf{q}',l'})-n^0(\epsilon_{\mathbf{q}+\mathbf{q}',l''})}{\epsilon_{\mathbf{q}+\mathbf{q}',l''}-\epsilon_{\mathbf{q}',l'}-\epsilon_{\mathbf{q},l}}\right\},\qquad(19)$$

where P indicates that the principal value is taken in a summation and the formal definitions of the W factors are as in Ref. 10. The above result refers to the energy shift for the discrete SW corresponding to mode l and in-plane wave vector $\mathbf{k}$, and the temperature dependence arises through the Bose factors $n^0(\epsilon_{\mathbf{q}',l'})$ representing the number of thermally excited SW with energy $\epsilon_{\mathbf{q}',l'}$.

The corresponding three-magnon damping contribution for the SW modes is found to be

$$\Gamma_{\mathbf{q},l}=-\pi\sum_{\mathbf{q}'l'l''}\{W_d[n^0(\epsilon_{\mathbf{q}',l'})+n^0(\epsilon_{\mathbf{q}-\mathbf{q}',l''})+1]$$
$$\times\delta(\epsilon_{\mathbf{q}-\mathbf{q}',l''}+\epsilon_{\mathbf{q}',l'}-\epsilon_{\mathbf{q},l})+W_e[n^0(\epsilon_{\mathbf{q}',l'})$$
$$-n^0(\epsilon_{\mathbf{q}+\mathbf{q}',l''})]\delta(\epsilon_{\mathbf{q}+\mathbf{q}',l''}-\epsilon_{\mathbf{q}',l'}-\epsilon_{\mathbf{q},l})\},\qquad(20)$$

where the terms proportional to the Dirac delta functions $\delta(\epsilon_{\mathbf{q}-\mathbf{q}',l''}+\epsilon_{\mathbf{q}',l'}-\epsilon_{\mathbf{q},l})$ and $\delta(\epsilon_{\mathbf{q}+\mathbf{q}',l''}-\epsilon_{\mathbf{q}',l'}-\epsilon_{\mathbf{q},l})$ correspond to three-magnon splitting and confluence processes, respectively.

In the low-temperature limit of $T\to 0$, the above results simplify because the Bose factors terms vanish leaving

$$\Delta\epsilon_{\mathbf{q},l}(T=0)=P\sum_{\mathbf{q}'l'l''}\left(\frac{W_c}{\epsilon_{-\mathbf{q}-\mathbf{q}',l''}+\epsilon_{\mathbf{q}',l'}+\epsilon_{\mathbf{q},l}}\right)\qquad(21)$$

and

$$\Gamma_{\mathbf{q},l}(T=0)=-\pi\sum_{\mathbf{q}'l'l''}W_d\delta(\epsilon_{\mathbf{q}-\mathbf{q}',l''}+\epsilon_{\mathbf{q}',l'}-\epsilon_{\mathbf{q},l}).\qquad(22)$$

In particular, only the three-magnon splitting processes contribute to the SW damping in the low-temperature limit.

IV. FOUR-MAGNON PROCESSES

We next consider the terms in the Hamiltonian containing products of four creation or annihilation operators, following a similar procedure to that in the previous section. Some four-magnon terms occur even in the special case of a Heisenberg antiferromagnet, but additional contributions in our case come from the dipolar interactions. The $H^{(4)}$ term, when written in the representation with in-plane (2D) wave vectors and layer indices, becomes

$$H_1^{(4)}=\frac{1}{2}\sum_{\mathbf{k}_1,\mathbf{k}_2,\mathbf{q},n,n'}[M^{(4)}_{n,n'}(\mathbf{k}_1)c^\dagger_{\mathbf{k}_2,n}c^\dagger_{\mathbf{q}-\mathbf{k}_2,n}c_{\mathbf{q}-\mathbf{k}_1,n}c_{\mathbf{k}_1,n'}$$
$$+M^{(4)}_{n,n'}(-\mathbf{k}_2)c^\dagger_{\mathbf{k}_2,n'}c^\dagger_{\mathbf{q}-\mathbf{k}_2,n}c_{\mathbf{q}-\mathbf{k}_1,n}c_{\mathbf{k}_1,n'}$$
$$-2M'^{(4)}_{n,n'}(\mathbf{k}_1-\mathbf{k}_2)c^\dagger_{\mathbf{k}_2,n'}c^\dagger_{\mathbf{q}-\mathbf{k}_2,n}c_{\mathbf{q}-\mathbf{k}_1,n}c_{\mathbf{k}_1,n'}$$
$$+F'^{(4)}_{n,n'}(\mathbf{k}_1)c^\dagger_{\mathbf{q},n}c_{\mathbf{q}-\mathbf{k}_1-\mathbf{k}_2,n}c_{\mathbf{k}_2,n}c_{\mathbf{k}_1,n'}$$
$$+G'^{(4)}_{n,n'}(-\mathbf{k}_1)c^\dagger_{\mathbf{k}_1,n'}c^\dagger_{\mathbf{k}_2,n}c^\dagger_{\mathbf{q}-\mathbf{k}_1-\mathbf{k}_2,n}c_{\mathbf{q},n}],\qquad(23)$$

where

$$M^{(4)}_{n,n'}(\mathbf{k}_1) = -\frac{1}{2}\Big[v_{n,n-1}(\mathbf{q})\,\delta_{n,n-1} + v_{n,n+1}(\mathbf{q})\,\delta_{n,n+1} - \mu_{n,n'}\frac{(g\mu_B)^2}{4} D^{zz}_{n,n'}(\mathbf{q})\Big]$$

$$M'^{(4)}_{n,n'}(\mathbf{k}_1) = -\Big[v_{n,n-1}(\mathbf{q})\,\delta_{n,n-1} + v_{n,n+1}(\mathbf{q})\,\delta_{n,n+1} - (-1)^{\mu_{n,n'}}\frac{(g\mu_B)^2}{2} D^{zz}_{n,n'}(\mathbf{q})\Big]$$

$$F'^{(4)}_{n,n'}(\mathbf{k}_1) = \frac{\mu_{n,n'}}{8}(g\mu_B)^2[D^{xx}_{n,n'}(\mathbf{q}) - D^{yy}_{n,n'}(\mathbf{q}) - 2iD^{xy}_{n,n'}(\mathbf{q})]$$

$$G'^{(4)}_{n,n'}(\mathbf{k}_1) = \frac{\mu_{n,n'}}{8}(g\mu_B)^2[D^{xx}_{n,n'}(\mathbf{q}) - D^{yy}_{n,n'}(\mathbf{q}) + 2iD^{xy}_{n,n'}(\mathbf{q})], \tag{24}$$

and we have defined the function

$$\mu_{n,n'} \equiv \frac{3+(-1)^{n-n'}}{2}. \tag{25}$$

We then apply the canonical transformation (see Sec. II) to reexpress the above in terms of the α and $\alpha^\dagger$ operators, giving

$$H^{(4)} = \frac{1}{2}\sum_{l_1 l_2 l_3 l_4 \mathbf{k},\mathbf{k}',\mathbf{q}} \{\Lambda_1 \alpha^\dagger_{\mathbf{k}' l_1}\alpha^\dagger_{\mathbf{q}-\mathbf{k}',l_2}\alpha_{\mathbf{q}-\mathbf{k},l_3}\alpha_{\mathbf{k},l_4} + \Lambda_2 \alpha^\dagger_{\mathbf{q}l_1}\alpha_{\mathbf{q}-\mathbf{k}-\mathbf{k}',l_2}\alpha_{\mathbf{k}',l_3}\alpha_{\mathbf{k},l_4} + \Lambda_3 \alpha^\dagger_{\mathbf{k}'_1}\alpha^\dagger_{\mathbf{k}',l_2}\alpha^\dagger_{\mathbf{q}-\mathbf{k}-\mathbf{k}',l_3}\alpha_{\mathbf{q},l_4} + \Lambda_4 \alpha^\dagger_{\mathbf{k}' l_1}\alpha^\dagger_{\mathbf{q}-\mathbf{k}',l_2}\alpha^\dagger_{\mathbf{k}-\mathbf{q},l_3}\alpha^\dagger_{-\mathbf{k},l_4} + \Lambda_5 \alpha_{-\mathbf{k}' l_1}\alpha_{\mathbf{k}'-\mathbf{q},l_2}\alpha_{\mathbf{q}-\mathbf{k},l_3}\alpha_{\mathbf{k},l_4}\}, \tag{26}$$

where the amplitude factors, denoted by Λ_i ($i=1,2,\ldots,5$), associated with each operator term are again formally defined as in the ferromagnetic film case.[10] These terms can be represented diagrammatically and, by contrast with the three-magnon case, the four-magnon interactions vertices have an even number (four) incoming and outgoing SW Green's function lines. In general, the interactions Λ_i involve both dipolar and exchange contributions.

The leading-order contribution of the four-magnon processes to the self-energy comes from a diagram that is of first order in one of the interaction vertices, as shown in Fig. 2(b). It is found to be real for all values of the SW energy, and hence it provides a renormalization of the SW energy of each branch (but no damping term). Following Ref. 10, the energy shift associated with SW branch l at wave vector $\mathbf{q}$ is found to be

$$\Delta\epsilon_{\mathbf{q},l} = \sum_{\mathbf{q}'l'} \Theta_a n^0(\epsilon_{\mathbf{q}',l'}), \tag{27}$$

where the weighting term Θ_a are related to a combination of the Λ_1 vertices, as specified in Ref. 10.

In order to calculate the damping (which is related to the imaginary part of the self-energy), it is necessary to consider the contributions that are of second order in the four-magnon Λ_i vertices. Following the same formal procedure as for ferromagnetic films,[10] the final result for the damping of SW branch l due to four-magnon processes is

$$\Gamma_{\mathbf{q},l} = -\pi \sum_{\mathbf{q}',\mathbf{q}''l'l''l'''} \{\Theta_b\{n^0(\epsilon_{\mathbf{q}'-\mathbf{q},l'})[n^0(\epsilon_{\mathbf{q}'',l''})+1] - n^0(\epsilon_{\mathbf{q}'-\mathbf{q}'',l'''})[n^0(\epsilon_{\mathbf{q}'',l''}) - n^0(\epsilon_{\mathbf{q}'-\mathbf{q},l'})]\}\delta(\epsilon_{\mathbf{q}'',l''} + \epsilon_{\mathbf{q}'-\mathbf{q}'',l'''} - \epsilon_{\mathbf{q}'-\mathbf{q},l'} - \epsilon_{\mathbf{q},l}) + \Theta_c\{n^0(\epsilon_{\mathbf{q}'',l''})n^0(\epsilon_{\mathbf{q}'-\mathbf{q}'',l'''}) + [n^0(\epsilon_{\mathbf{q}'',l''})+1][n^0(\epsilon_{\mathbf{q}'',l''}) + n^0(\epsilon_{\mathbf{q}'-\mathbf{q}'',l'''})+1]\} \times \delta(\epsilon_{\mathbf{q}'',l''} + \epsilon_{\mathbf{q}-\mathbf{q}',l'} + \epsilon_{\mathbf{q}'-\mathbf{q}'',l'''} - \epsilon_{\mathbf{q},l}) + \Theta_d\{n^0(\epsilon_{\mathbf{q}'-\mathbf{q},l'})[n^0(\epsilon_{\mathbf{q}'',l''})+1] - n^0(\epsilon_{\mathbf{q}'-\mathbf{q},l'})[n^0(\epsilon_{\mathbf{q}'',l''}) - n^0(\epsilon_{\mathbf{q}'-\mathbf{q},l'})]\}\delta(\epsilon_{\mathbf{q}'+\mathbf{q}'',l'''} - \epsilon_{\mathbf{q}'',l''} - \epsilon_{\mathbf{q}'-\mathbf{q},l'} - \epsilon_{\mathbf{q},l})\}. \tag{28}$$

Here the weighting factors $\Theta_{a,b,c,d}$, are formally identical to the ones described in Ref. 10.

V. NUMERICAL APPLICATIONS

We now present numerical calculations for the damping and renormalization of the SW modes in antiferromagnetic thin films, based on expressions obtained in the previous sections. We employ parameters appropriate to the rutile-structure antiferromagnet MnF_2 ($T_N = 68$ K, $S = \frac{5}{2}$), where the magnetic ions form a body-centered tetragonal lattice. In this case the parameters of the sublattice magnetization, exchange constant, and effective anisotropy field are known from previous work.[6] For relatively large N (where N is the total number of magnetic layers) of the order of 100 or more, the predictions for the *linear* SW spectrum are consistent

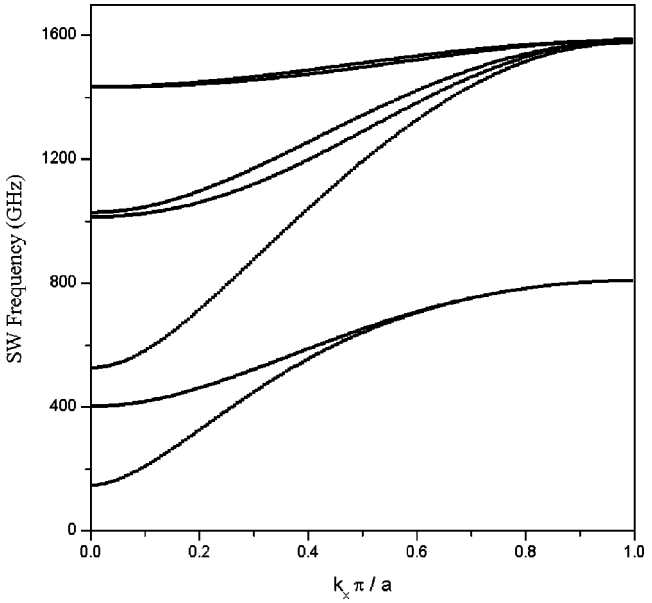

FIG. 3. Dipole-exchange SW dispersion relations for a MnF_2 antiferromagnetic film with seven atomic layers.

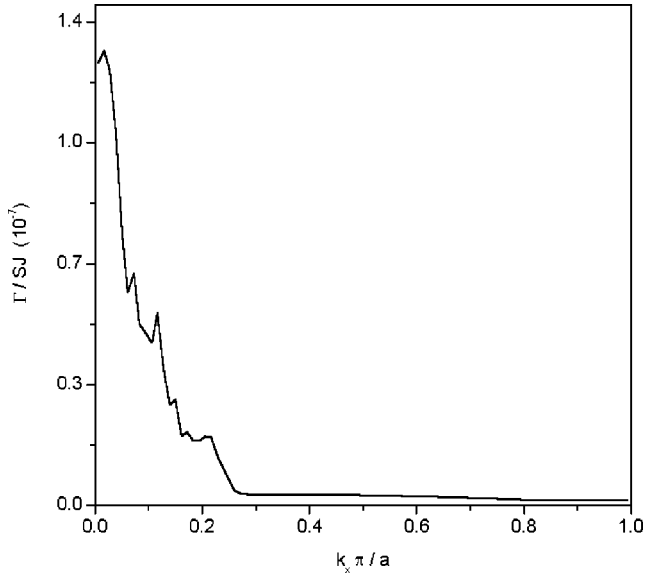

FIG. 5. Three-magnon damping (relative to SJ) versus reduced wave vector of the second-lowest SW branch ($l=2$) in an ultrathin film with seven layers.

with those carried out for films using a continuum dipole-exchange approach[6] with Maxwell's equations describing the dipolar terms. For ultrathin films the discrete nature of the SW spectrum becomes apparent and also there is a symmetry difference depending on whether N is odd or even. In the former case there are more layers of one sublattice type than the other, giving a net magnetization field. However, when N is even, the static magnetizations of the two sublattices cancel out. This leads to a greater splitting between modes in the case of N odd. Figures 3 and 4 show examples of the linear spectrum of the dipole-exchange SW modes for ultrathin MnF_2 films with seven and eight layers, respectively.

In order to evaluate numerically the SW energy shift and damping from three-magnon processes, the wave vector summations in Eqs. (19)–(22) are performed over discrete values in the 2D Brillouin zone. Specifically, the wave-vector labels are taken from a lattice of $L\times L$ points in the Brillouin zone. In our case, a typical calculation employed lattices with 200×200 points, for wave vectors ranging from $-\pi/a$ to $+\pi/a$ in both the x and z components of the in-plane wave vector. The weighting factors are obtained by numerically evaluating the elements of the transformation matrix $\mathcal{S}_{\mathbf{q}}$ at each point in the lattice. This procedure involves the direct inversion of a $2N\times 2N$ matrix. The final results for the damping and energy shift shown below are then calculated as a function of the external wave vector chosen as $\mathbf{q}=(q_x,0)$. Other propagation directions for $\mathbf{q}$ may similarly be studied.

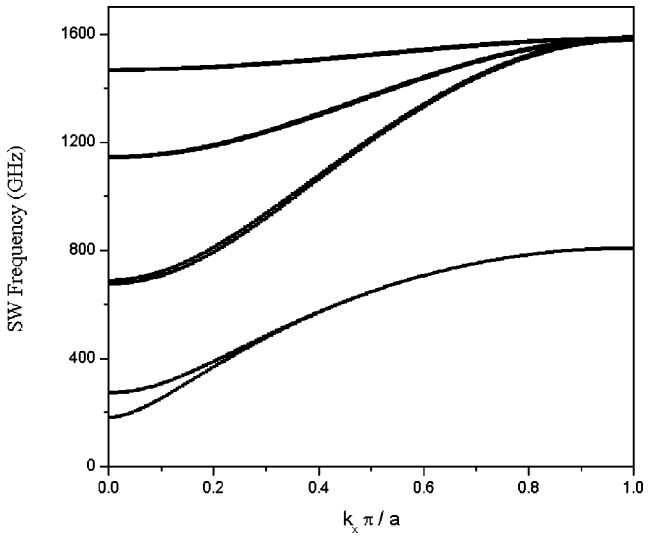

FIG. 4. Dipole-exchange SW dispersion relations for a MnF_2 antiferromagnetic film with eight atomic layers.

In the case of the three-magnon SW damping, the summations in Eq. (19) must take into account the energy and 2D wave vector conservation conditions implicit in the δ functions. For the numerical evaluations the delta functions were approximated by sharply peaked Lorentzian functions. For the calculation of the energy shift, where there are no δ function terms, it was found to be important to include the contributions from *all* the different processes (i.e., the terms representing all combinations of l' and l'' SW branch labels) in determining the principal part of the summations. For a film with N layers, that means that the energy shift corresponds to the sum of N^2 different contributions. However, in the case of damping we find that only a relatively few (l',l'') terms contribute significantly, because of the restrictions due to the δ functions.

In Fig. 5 we show some results for the damping due to the dominant three-magnon processes in MnF_2 in the low-temperature limit. This calculation is for SW branch 2 (we label the modes in increasing magnitude in terms of their frequencies at $\mathbf{q}=0$) for an ultrathin film with seven atomic layers. The graph shows the relative damping Γ/SJ in terms of the in-plane wave-vector component q_x, for SW's propagating along the x crystallographic direction (see Fig. 1 for

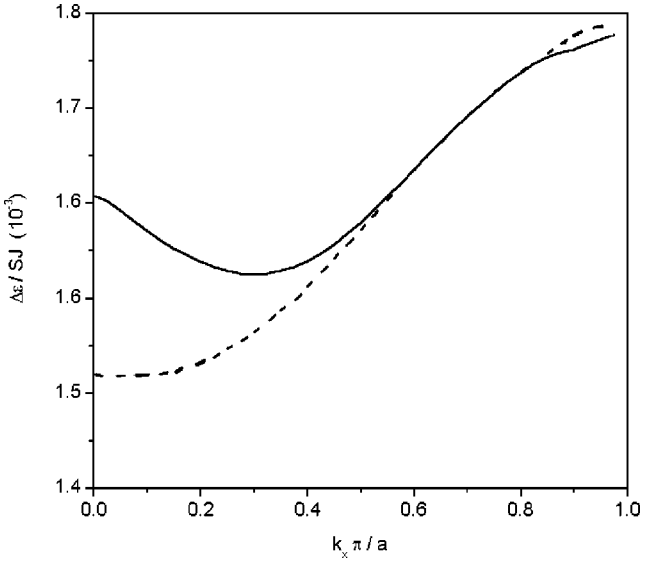

FIG. 6. Three-magnon energy shift (relative to SJ) versus reduced wave vector of the two lowest frequency branches, $l=1$ (solid line) and $l=2$ (dashed line), in a thin film with seven layers.

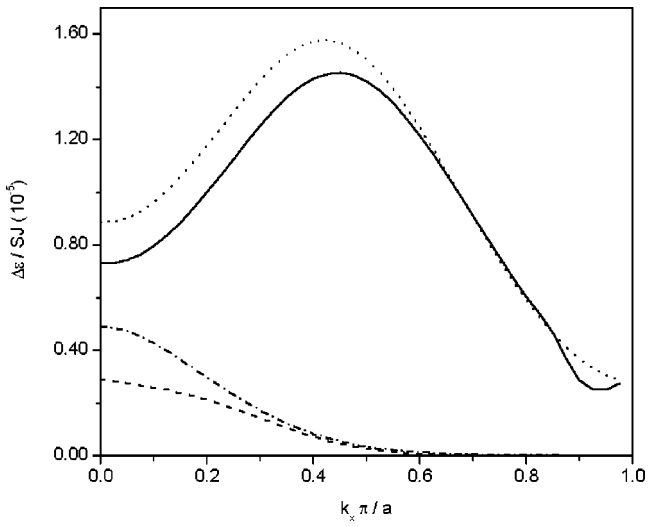

FIG. 7. Contributions to the three-magnon energy shift (relative to SJ) of some individual interaction processes in the case of $N=7$ and branch $l=1$: (1,1)—solid line, (1,2)—dotted line, (3,3)—dot-dashed line, and (4,4)—dashed line.

the film geometry). The main contribution to the damping, in this case, comes from the $l'=l''=1$ temperature-independent splitting process. This corresponds to the terms multiplied by the weighting factor W_d in Eq. (20). The contribution of the confluence processes is found to be negligible for $T \ll T_c$ in this example. This can be explained by the small magnitude of the Bose occupation factors in the expressions for the confluence processes, in that temperature range. The graph shows that the damping has its maximum in a small wave vector region, with a cut-off for larger values of q_x (for $N=7$, the cutoff happens at $q_x a/\pi \approx 0.25$). This (and other sharp features in the graph, are a consequence of the δ functions in the expressions for the damping. These δ functions, which express the frequency and momentum conservation conditions, impose restrictions on the interaction processes that are allowed to contribute to the damping, and are also responsible for the existence of peaks and structural features in the results, as can be seen in the figures. We also found a decrease in the magnitude of the damping as the number of layers in the film is increased. Both of these effects may be attributed to the fact that, for larger N, the modes are closer together, thereby influencing how the delta functions can be satisfied.

The corresponding energy shifts due to three-magnon processes for the two lowest ($l=1$ and $l=2$) modes in the same seven-layer film are shown in Fig. 6. The results are plotted in terms of $\Delta\epsilon/SJ$ versus wave vector. Although the relative energy shift for mode 2 (broken line) is smaller than that for mode 1 (solid line) at small wave vectors, the energy shifts tend to become the same for larger wave vectors. This behavior occurs because the splitting between SW branches 1 and 2 (see Fig. 3) becomes less important for larger wave vectors. The results shown in Fig. 6 are the sum of the contributions from all the processes (49 in this case), which are associated with the different combinations of l' and l'' internal branch labels. This is illustrated in Fig. 7 where we show the contributions from some individual (l',l'') processes to the energy shift of branch 1, namely, processes (1,1), (1,2), (3,3), and (4,4).

Our results point to a strong effect on the damping of the SW modes depending on whether N is even or odd. This is particularly apparent for the damping of the lowest two branches when N is relatively small. It is related to our earlier discussion of the linear SW spectra (see Figs. 3 and 4 for N equal to 7 and 8, respectively). For small wave vectors the resulting imbalance in the sublattice magnetizations (when N is odd) leads to larger splitting of the lowest SW branches compared with the even N case. A consequence is that the δ-function conditions, requiring energy and 2D-momentum conservation, for the three-magnon splitting processes are more readily satisfied when N is odd. We have already illustrated this with the damping for mode 2 in the case of $N=7$ in Fig. 5. In contrast, when N is small and even (for example, $N=8$ as in Fig. 4), we find that the damping of mode 2 is very much smaller (by a factor of at least 10) due to the much smaller splitting between SW modes 1 and 2 in this case. These differences between the even and odd cases tend to become negligible for thicker films ($N \to \infty$), as expected.

Next we briefly consider the four-magnon interaction processes. Some results for the four-magnon energy shift as a function of wave vector are presented in Fig. 8 for MnF_2 films with three different thicknesses: $N=7$ (solid line), $N=8$ (dashed line), and $N=9$ (dot-dashed line). Again, in this case, one can observe an even-odd property whereby the number of layers also influences the energy shift, with the results for $N=8$ being much smaller than for either $N=7$ or $N=9$ over a wide range of wave vectors. These results are deduced from Eq. (27) for a fixed value of temperature. We have also considered the effect of varying the temperature on the renormalization of the SW modes. Figure 9 shows the calculated temperature dependence of the four-magnon energy shift for two different values of the in-plane wave vec-

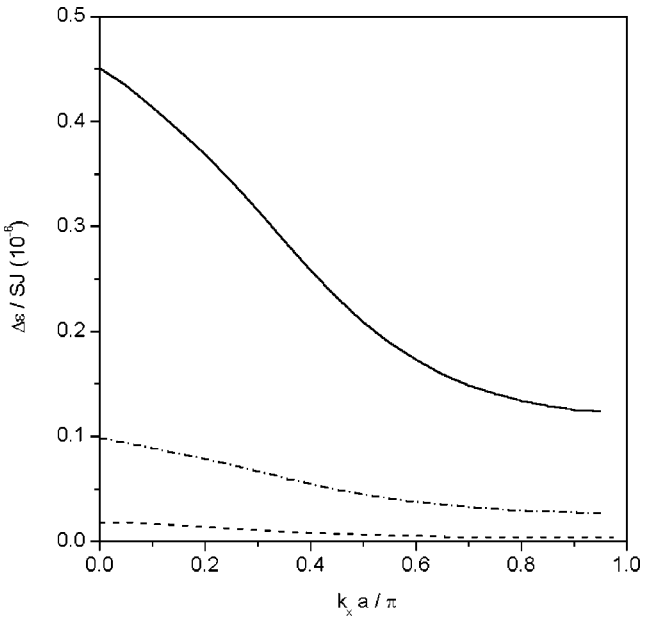

FIG. 8. Four-magon energy shift (relative to SJ) versus reduced wave vector for the lowest SW branch $l=1$ of films with seven (solid line), eight (dot-dashed line), and nine (dashed line) atomic layers. The temperature corresponds to $k_BT/SJ=0.5$.

tor component: $k_x=0.1\pi/a$ and $k_x=0.5\pi/a$. Due to the thermal population factor in Eq. (27), the energy shift increases rapidly with temperature, especially if k_BT starts to become comparable with SJ (implying that T approaches T_N, which is beyond the range of validity of the theory). However, even then, the contributions are still small compared to the three-magnon results (see Fig. 6), which in turn are dominated by the temperature-independent contribution. Likewise, the four-magnon contribution to the damping is

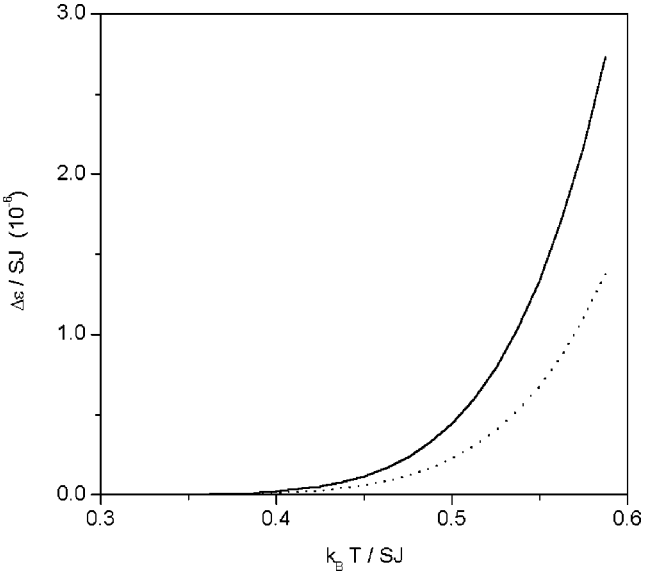

FIG. 9. Four-magnon energy shift (relative to SJ) for the lowest SW branch $l=1$ versus temperature for a film with seven layers and two different wave vectors: $k_xa/\pi=0.5$ (solid line) and $k_xa/\pi=0.1$ (dotted line).

estimated to be small compared to the three-magnon contribution in the case of ultrathin MnF_2 films. This is mainly because of the double wave-vector summations in Eq. (28), together with the thermal factors.

VI. CONCLUSIONS

We have developed a diagrammatic perturbation formalism for the Green's functions that describe the dipole-exchange SW dynamics in antiferromagnetic ultrathin films. This Hamiltonian-based microscopic formalism was obtained as an extension of a previous calculation for ferromagnetic films, and allowed us to find results for the damping and energy shift of magnons due to three-magnon and four-magnon interaction processes involving combinations of the discrete SW modes. Qualitative differences compared to the case of bulk materials[11,12] occur because of this discrete aspect of the SW spectrum, e.g., the appearance of additional peaks and structure in the three-magnon damping results in Sec. V. The formalism was applied to ultrathin films of the rutile MnF_2 antiferromagnet. The results point to a strong dependence of the nonlinear processes on the number of layers in the films. In particular, both the damping and renormalization of the SW frequencies can be significantly influenced by the even-odd aspect of the total number of layers. This effect certainly is a consequence of the nonequivalence of the sublattices that occurs in films with an odd number of layers. It could, in principle, be investigated by experimental techniques such as inelastic light scattering.[13,14] An interesting theoretical extension of the present work would be to investigate antiferromagnets with other crystal structures, as well as films with different crystal orientations.[15]

There are, of course, other processes, apart from the three- and four-magnon interactions, that may contribute to the total SW damping in antiferromagnets. For example, these include damping due to impurities and defects (in the surface or bulk of the film) and spin-phonon interactions. To some extent the different processes might be distinguished experimentally from one another by their different behavior with respect to varying the 2D in-plane wave vector, temperature, and applied magnetic field.

ACKNOWLEDGMENTS

The authors acknowledge financial support from the agencies NSERC (Canada), CAPES (Brazil), and CNPq (Brazil).

APPENDIX

The $H^{(2)}$ term in the Hamiltonian is given by Eq. (10) in the $(\mathbf{k},n)$ representation where layer index $n=1,2,\ldots,N$. We now define the following $N\times 1$ matrices (N being the number of layers in the film):

$$\mathbf{c}_\mathbf{k}^\dagger=\begin{pmatrix} c_{\mathbf{k}1}^\dagger \\ c_{\mathbf{k}2}^\dagger \\ \vdots \\ c_{\mathbf{k}N}^\dagger \end{pmatrix}, \quad \mathbf{c}_\mathbf{k}=\begin{pmatrix} c_{\mathbf{k}1} \\ c_{\mathbf{k}2} \\ \vdots \\ c_{\mathbf{k}N} \end{pmatrix}. \tag{A1}$$

Thus, we can rewrite the Hamiltonian term as

$$H^{(2)}=\sum_{\mathbf{k}}\ \{\tilde{\mathbf{c}}_{\mathbf{k}}^{\dagger}\mathbf{M}(\mathbf{k})\mathbf{c}_{\mathbf{k}}+\tilde{\mathbf{c}}_{\mathbf{k}}\mathbf{N}(\mathbf{k})\mathbf{c}_{-\mathbf{k}}+\tilde{\mathbf{c}}_{\mathbf{k}}^{\dagger}\mathbf{N}(\mathbf{k})\mathbf{c}_{-\mathbf{k}}^{\dagger}\}, \tag{A2}$$

where $\mathbf{M}(\mathbf{k})$ and $\mathbf{N}(\mathbf{k})$ are $N\times N$ matrices with elements $M_{n,n'}(\mathbf{k})$ and $N_{n,n'}(\mathbf{k})$, respectively, and the tilde represents the transpose. We also define column matrices with $2N$ components

$$\mathcal{C}_{\mathbf{k}}^{\dagger}=\begin{pmatrix}\mathbf{c}_{\mathbf{k}}^{\dagger}\\ \mathbf{c}_{-\mathbf{k}}\end{pmatrix},\quad \mathcal{C}_{\mathbf{k}}=\begin{pmatrix}\mathbf{c}_{\mathbf{k}}\\ \mathbf{c}_{-\mathbf{k}}^{\dagger}\end{pmatrix}. \tag{A3}$$

After some straightforward but lengthy algebra, $H^{(2)}$ may be rewritten in a more compact form as

$$H^{(2)}=-\frac{1}{2}\sum_{\mathbf{k},n}\ M_{n,n}(\mathbf{k})(-1)^n+\frac{1}{2}\mathcal{H}^{(2)}, \tag{A4}$$

where

$$\mathcal{H}^{(2)}=\sum_{k}\ \tilde{\mathcal{C}}_k^{\dagger}\boldsymbol{\chi}(\mathbf{k})\mathcal{C}_k \tag{A5}$$

and $\boldsymbol{\chi}(\mathbf{k})$ is a $2N\times 2N$ matrix:

$$\boldsymbol{\chi}(\mathbf{k})=\begin{pmatrix}\mathbf{M}(\mathbf{k}) & 2\mathbf{N}(\mathbf{k})\\ 2\mathbf{N}(-\mathbf{k}) & \tilde{\mathbf{M}}(-\mathbf{k})\end{pmatrix}. \tag{A6}$$

The next step (before developing a diagrammatic perturbation method) is to simplify $H^{(2)}$ by transforming to a representation in which the matrix $\boldsymbol{\chi}(\mathbf{k})$ is diagonalized. This will have the effect of ''picking out'' the linear SW modes. We recall that in the antiferromagnetic film with N layers there are N SW modes, and these occur in doubly degenerate pairs in our $2N\times 2N$ matrix representation. We assign an index ν $(=1,2,\ldots,N)$ to each mode energy $\boldsymbol{\epsilon}_{\nu}$, and then perform a simple canonical transformation on the boson creation and annihilation operators that diagonalize $\mathcal{H}^{(2)}$. The required transformation (to new boson operators) is defined by

$$\mathcal{C}_{\mathbf{k}}^{\dagger}=\mathcal{S}_{\mathbf{k}}^{*}\mathbf{A}_{\mathbf{k}}^{\dagger},$$

$$\mathcal{C}_{\mathbf{k}}=\mathcal{S}_{\mathbf{k}}\mathbf{A}_{\mathbf{k}}, \tag{A7}$$

with the notation

$$\mathbf{A}_{\mathbf{k}}^{\dagger}=\begin{pmatrix}\boldsymbol{\alpha}_{\mathbf{k}}^{\dagger}\\ \boldsymbol{\alpha}_{-\mathbf{k}}\end{pmatrix},\quad \mathbf{A}_{\mathbf{k}}=\begin{pmatrix}\boldsymbol{\alpha}_{\mathbf{k}}\\ \boldsymbol{\alpha}_{-\mathbf{k}}^{\dagger}\end{pmatrix}. \tag{A8}$$

We seek a diagonalized Hamiltonian with the form

$$\mathcal{H}^{(2)}=\sum_{\mathbf{k}}\ \begin{pmatrix}\tilde{\boldsymbol{\alpha}}_{\mathbf{k}}^{\dagger} & \tilde{\boldsymbol{\alpha}}_{-\mathbf{k}}\end{pmatrix}\begin{pmatrix}\boldsymbol{\varepsilon}(\mathbf{k}) & 0\\ 0 & \boldsymbol{\varepsilon}(\mathbf{k})\end{pmatrix}\begin{pmatrix}\boldsymbol{\alpha}_{\mathbf{k}}\\ \boldsymbol{\alpha}_{-\mathbf{k}}^{\dagger}\end{pmatrix}, \tag{A9}$$

where the $N\times N$ diagonal matrix $\boldsymbol{\varepsilon}(\mathbf{k})$ of SW energies is

$$\boldsymbol{\varepsilon}(\mathbf{k})=\begin{pmatrix}\epsilon_1(\mathbf{k}) & \ldots & 0\\ \vdots & \ddots & \vdots\\ 0 & \ldots & \epsilon_N(\mathbf{k})\end{pmatrix}. \tag{A10}$$

In other words, we want to find a transformed $\boldsymbol{\chi}(\mathbf{k})$ as

$$\boldsymbol{\chi}(\mathbf{k})\rightarrow\begin{pmatrix}\boldsymbol{\varepsilon}(\mathbf{k}) & 0\\ 0 & \boldsymbol{\varepsilon}(\mathbf{k})\end{pmatrix}, \tag{A11}$$

whereupon we can then rewrite Eq. (A5) as

$$\mathcal{H}^{(2)}=\sum_{\mathbf{k}}\ \mathrm{Tr}[\boldsymbol{\varepsilon}(\mathbf{k})]+2\sum_{\mathbf{k}}\ \tilde{\boldsymbol{\alpha}}_{\mathbf{k}}^{\dagger}\boldsymbol{\varepsilon}(\mathbf{k})\boldsymbol{\alpha}_{\mathbf{k}}, \tag{A12}$$

and the original Hamiltonian (A4) becomes

$$H^{(2)}=-\frac{1}{2}\sum_{\mathbf{k},n}\ [M_{n,n'}(\mathbf{k})(-1)^n-\boldsymbol{\varepsilon}(\mathbf{k})]\delta_{n,n'}$$

$$+\sum_{\mathbf{k},\nu}\ \boldsymbol{\epsilon}_{\nu}(\mathbf{k})\alpha_{\mathbf{k},\nu}^{\dagger}\alpha_{\mathbf{k},\nu}. \tag{A13}$$

Finally, we specify how the transformation matrix $\mathcal{S}_k$ can be calculated. From Eqs. (A7) and (A11) we have the requirement that the transformed $\boldsymbol{\chi}(\mathbf{k})$ matrix satisfies

$$\tilde{\mathcal{S}}_{\mathbf{k}}^{*}\boldsymbol{\chi}(\mathbf{k})\mathcal{S}_{\mathbf{k}}=\begin{pmatrix}\boldsymbol{\varepsilon}(\mathbf{k}) & 0\\ 0 & \boldsymbol{\varepsilon}(\mathbf{k})\end{pmatrix}. \tag{A14}$$

We also use the property that the α and $\alpha^{\dagger}$ operators obey boson commutation relations, which in matrix form is expressed as

$$\mathbf{A}_{\mathbf{k}}\tilde{\mathbf{A}}_{\mathbf{k}}^{\dagger}-(\mathbf{A}_{\mathbf{k}}^{\dagger}\tilde{\tilde{\mathbf{A}}}_{\mathbf{k}})=\begin{pmatrix}\mathbf{I} & 0\\ 0 & \mathbf{I}\end{pmatrix}, \tag{A15}$$

where $\mathbf{I}$ is the $N\times N$ unit matrix. We thus obtain

$$\mathcal{S}_{\mathbf{k}}\begin{pmatrix}\mathbf{I} & 0\\ 0 & -\mathbf{I}\end{pmatrix}\tilde{\mathcal{S}}_{\mathbf{k}}^{*}=\begin{pmatrix}\theta & 0\\ 0 & -\theta\end{pmatrix}, \tag{A16}$$

where θ is the $N\times N$ diagonal matrix with elements $\boldsymbol{\theta}_{n,n'}=(-1)^n\delta_{n,n'}$. Equation (A14) may then be rewritten as

$$\begin{pmatrix}\theta & 0\\ 0 & -\theta\end{pmatrix}\chi(\mathbf{k})\mathcal{S}_{\mathbf{k}}=\mathcal{S}_{\mathbf{k}}\begin{pmatrix}\boldsymbol{\varepsilon}(\mathbf{k}) & 0\\ 0 & -\boldsymbol{\varepsilon}(\mathbf{k})\end{pmatrix}. \tag{A17}$$

This result allows us to obtain the $\mathcal{S}_{\mathbf{k}}$ matrix provided $\chi(\mathbf{k})$ and $\varepsilon(\mathbf{k})$ are known. Writing $\mathcal{S}_{\mathbf{k}}=(S_{\mathbf{k},1},S_{\mathbf{k},2},\ldots,S_{\mathbf{k},2N})$, where each $S_{\mathbf{k},j}$ is a column matrix, we obtain

$$\begin{pmatrix}\theta & 0\\ 0 & -\theta\end{pmatrix}\chi(\mathbf{k})(S_{\mathbf{k},1},S_{\mathbf{k},2},\ldots,S_{\mathbf{k},2N})$$

$$=(S_{\mathbf{k},1},S_{\mathbf{k},2},\ldots,S_{\mathbf{k},2N})\begin{pmatrix}\boldsymbol{\varepsilon}(\mathbf{k}) & 0\\ 0 & -\varepsilon(\mathbf{k})\end{pmatrix}, \tag{A18}$$

which implies

$$\begin{pmatrix} \theta\mathbf{M}(\mathbf{k}) & 2\theta\mathbf{N}(\mathbf{k}) \\ -2\theta\mathbf{N}(-\mathbf{k}) & -\theta\tilde{\mathbf{M}}(-\mathbf{k}) \end{pmatrix} S_{\mathbf{k},j} = \pm \epsilon_j(\mathbf{k}) S_{\mathbf{k},j} . \tag{A19}$$

The plus sign is used here for $j \in \{1, \ldots, N\}$ and theminus sign for $j \in \{N+1, \ldots, 2N\}$. By solving Eq. (A19) for $S_{\mathbf{k},j}$ one can find the transformation matrix $\mathcal{S}_{\mathbf{k}}$ and thereby diagonalize the $H^{(2)}$ part of the Hamiltonian. This can be conveniently carried out numerically.

[1] *Ultrathin Magnetic Structures*, edited by B. Heinrich and J.A.C. Bland (Springer-Verlag, Berlin, 1994), Vols. I, II.

[2] *Linear and Nonlinear Spin Waves in Magnetic Films and Superlattices*, edited by M.G. Cottam (World Scientific, Singapore, 1994).

[3] S.O. Demokritov, B. Hillebrands, and A.N. Slavin, Phys. Rep. **348**, 442 (2001).

[4] R.P. Erickson and D.L. Mills, Phys. Rev. B **43**, 10 715 (1991).

[5] R.P. Erickson and D.L. Mills, Phys. Rev. B **44**, 11 825 (1991).

[6] F.C. Nortemann, R.L. Stamps, and R.E. Camley, Phys. Rev. B **47**, 11 910 (1993).

[7] J. Milton Pereira, Jr. and M.G. Cottam, J. Appl. Phys. **87**, 5941 (2000).

[8] H. Benson and D.L. Mills, Phys. Rev. **178**, 839 (1969).

[9] R.N. Costa Filho, M.G. Cottam, and G.A. Farias, Solid State Commun. **108**, 439 (1998).

[10] R.N. Costa Filho, M.G. Cottam, and G.A. Farias, Phys. Rev. B **62**, 6545 (2000).

[11] F. Keffer, in *Handbuch der Physik*, edited by S. Flüge (Springer-Verlag, Berlin, 1994), Vol. XVIII/B.

[12] V.S. L'vov, *Wave Turbulence Under Parametric Excitation* (Springer-Verlag, Berlin, 1994).

[13] M.G. Cottam and D. Kontos, J. Phys. C **13**, 2945 (1980).

[14] P. Grünberg, in *Light Scattering in Solids V*, edited by M. Cardona and G. Güntherhodt (Springer-Verlag, Berlin, 1989), p. 303.

[15] J.M. Pereira, Jr. and M.G. Cottam, Phys. Rev. B **63**, 174431 (2001).